Effect of Impact Velocity and Mass Ratio During Vertical Sphere Water Entry

Dillon Schwalbach[1], Thomas Shepard[2], Seamus Kane[3], David Siglin[4], Teegan Harrington[5], John Abraham[6]

School of Engineering, University of St. Thomas 2115 Summit Avenue, St. Paul, MN 55105, USA

[1]schw0284@stthomas.edu; [2]thomas.shepard@stthomas.edu; [3]kane9823@stthomas.edu; [4]sigl9148@stthomas.edu; [5]harr7950@stthomas.edu; [6]jpabraham@stthomas.edu

Abstract

The cavity formation and drag forces following spherical object impacts on a water free surface have been observed experimentally from the period of initial impact to cavity pinch-off. The impact velocity, sphere density, and surface wettability were varied while the diameter was held near-constant (39.3-39.9 mm). Impact velocity was varied between 2.4 m/s and 6.8 m/s and the sphere density was varied between 656 kg/m^3 and 6760 kg/m^3. Increasing impact velocity while keeping sphere density constant was shown to result in an deeper cavity pinch-off and a decrease in pinch-off time. Increasing sphere density while keeping impact velocity constant results in an increase in cavity pinch-off depth and pinch-off time. A correlation was observed between the ratio of the kinetic energy of the sphere and the surface tension of the water with the dimensionless depth of the cavity pinch-off, independent of surface wettability. The dimensionless time of the cavity pinch-off with respect to gravity was found to be near constant, and independent of sphere density, impact velocity, and surface wettability. The dimensionless time of the cavity pinch-off with respect to impact velocity was found to increase linearly with liquid Weber number.

Keywords

Water Impact Forces; Underwater Trajectory; Oceanography; Expendable Bathythermography; Water Cavity Formation; Hydrophilic Surfaces; Hydrophobic Surfaces

Introduction

The free surface water-entry characteristics of spherical objects have been examined through experimentation for over a century. Efforts to characterize the impact behavior have been improved with the acquisition of new technologies: first with the use of single-spark photography by Worthington and Cole (1897), high-speed digital video imaging, and numerical simulation. Past studies have focused on two major phenomena: the cavity behavior as a function of depth and time, and the drag force acting on the sphere as a function of depth and/or time. The present study examines how cavity dynamics and projectile acceleration are affected by varying the mass, surface contact angle, and impact velocity of the spherical body while holding the radius near-constant. Results are presented from initial water impact to cavity pinch-off.

To accurately characterize the descent of projectiles which pass from gaseous to liquid regions, the impact behaviour must be known. For instance, to correctly calculate ocean temperatures using eXpendable Bathy Thermographs (XBT), the period between the initial impact and the cavity pinch-off must be well understood. Within this narrow range of time, the descending object can undergo rapid changes in acceleration. Accounting for the effects of the impact would allow the depth of the XBT device, or other projectiles, to be determined more accurately than the current method which relies on a constant acceleration. With respect to oceanographic measurement devices such as the XBT, two recent studies have investigated the importance of the impact forces on their descent, Abraham et al. (2014) and Gorman et al. (2014). Prior to that, studies made conclusions on XBT descent included only fully submerged dynamic models, for example Stark et al. (2011), Abraham et al. (2011), Abraham et al. (2012a), Abraham et al. (2012b), and Abraham et al. (2013).

A surface contact angle of 90° demarcates two principle surface conditions; hydrophilic surfaces are characterized by a surface contact angle less than 90° and hydrophobic surfaces are characterized by a surface contact angle greater than 90°. In the *deep-seal* cavity regime, where the cavity collapses at a location between the descending object and the free surface, cavity behavior may be characterized by the depth and time at which cavity pinch-off occurs, as observed by Aristoff & Bush (2009). In Fig. 1, a series of images illustrates the cavity formed behind the impacting

sphere at the moments surrounding the cavity pinch-off event in the deep-seal regime.

The surface contact angle of the impacting sphere determines a critical impact velocity for cavity formation, as observed by Aristoff & Bush (2009), Duclaux et al. (2007), Duez, Ybert, Clanet, and Bocquet (2007), May (1975), and Truscott, Epps, and Techet (2012). Duez et al. (2007) further concluded that the liquid viscosity and surface tension also affect the threshold velocity for cavity formation. Interestingly, Duez et al. reported that sphere diameter does not effect the critical velocity while May (1951) demonstrated that sphere diameter can affect the threshold velocity for cavity formation for spheres with diameters below 1 inch. Larger spheres were seen to have a higher critical velocity. Furthermore, May (1951) concluded that the density of the impacting sphere does not affect the threshold velocity for cavity formation. Aristoff and Bush (2009) presented a map of various cavity regime classifications for spheres that demonstrates how the type of cavity which forms is impacted by the Bond and Weber numbers.

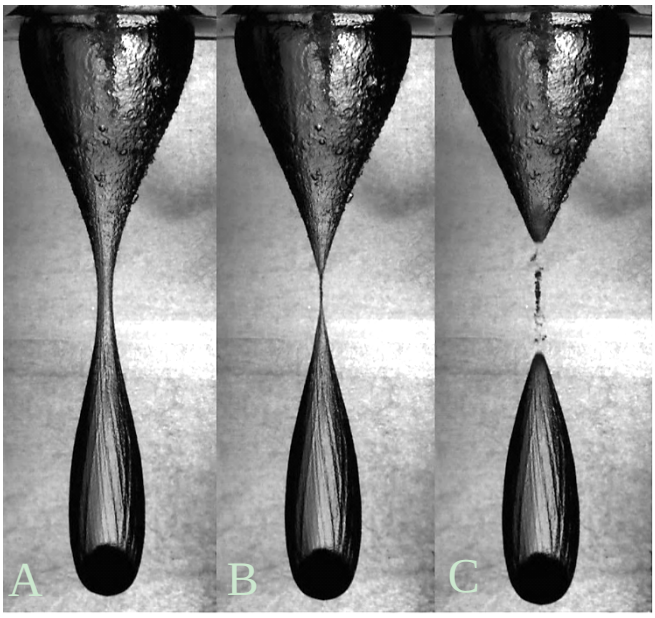

FIG. 1: A SERIES OF IMAGES SHOWING (A) 0.926 MS BEFORE CAVITY PINCH-OFF, (B) THE MOMENT OF CAVITY PINCH-OFF, AND (C) 0.926 ms AFTER CAVITY PINCH-OFF FOR A SPHERE WITH D = 39.86 mm, M = 218 g, U_O = 6.37 m/s, AND Θ = 115°

Duclaux et al. (2007) found that the dimensionless depth of the cavity pinch-off increases linearly with the impact velocity for a fixed sphere diameter. Additionally, Duclaux et al. (2007) observed a decrease in the dimensionless pinch-off depth of the cavity as the diameter of the sphere was increased for a constant impact velocity. May (1952) and Lee, Longoria, and Wilson (1996) concluded that for a given impacting sphere radius, the time at which the cavity pinches off is independent of impact velocity. Additionally, Lee, Longoria, and Wilson (1996) noted that the depth of the cavity pinch-off has a weak dependence on impact velocity. Truscott, Epps, and Techet (2012) conclude that the depth of cavity pinch-off exhibits a positive relationship to the mass-ratio of the impacting sphere and fluid, and the non-dimensional time to cavity pinch-off is constant.

Truscott, Epps, and Techet (2012) also observed a significant decrease in the acceleration of the impacting sphere immediately prior to the cavity pinch-off event. Additionally, they noted that the presence of a cavity decreases the hydrodynamic force coefficient of the impacting sphere. Baldwin & Steves (1975) concluded that for the early stages of water entry, the density and weight of the impacting sphere have no effect on the hydrodynamic forces. In addition to these discussions of cavity dynamics, detailed discussions of impact drag force have recently been reported in Abraham et al. (2014) and Gorman et al., (2014).

In a seminal review of the literature on the water entry of projectiles Truscott, Epps and Belden (2013) state that effect of mass ratio has "largely been ignored in the literature." The mass ratio (m*) is the ratio of the sphere density to water density (sphere mass to the mass of displaced water). One aim of this study is to better understand the effect of mass ratio on cavity dynamics and sphere acceleration during impact. The density ratio between the sphere and the water was varied between 0.66 to 6.8 with five different values. To better detect the influence of impact velocity, the impact velocity (U_o) was varied between 2.44 m/s and 6.77 m/s by dropping each sphere from six different heights. Additionally, hydrophobic and hydrophilic surfaces were created for each density ratio value. Therefore, sixty discrete experimental conditions were observed. By independently varying the impact velocity, the density ratio, and the surface contact angle of the sphere, this study obtained data within a range which was not covered by previous studies. These experimental conditions are considered low-speed or very low-speed water entries which occur for low Froude numbers, Fr < 70, where $Fr = U_o^2/gD$. One hallmark of these low-speed entries is the development of a deep-seal cavity which collapses and pinches off while the top portion is still open to the atmosphere at the surface of the water (Fig. 1).

Experimental Methods

In order to capture information on the cavity dynamics and forces acting on the sphere during water entry, a high-speed camera system recorded images during the impact and cavity closure process. The experimental set-up is shown in Fig. 2.

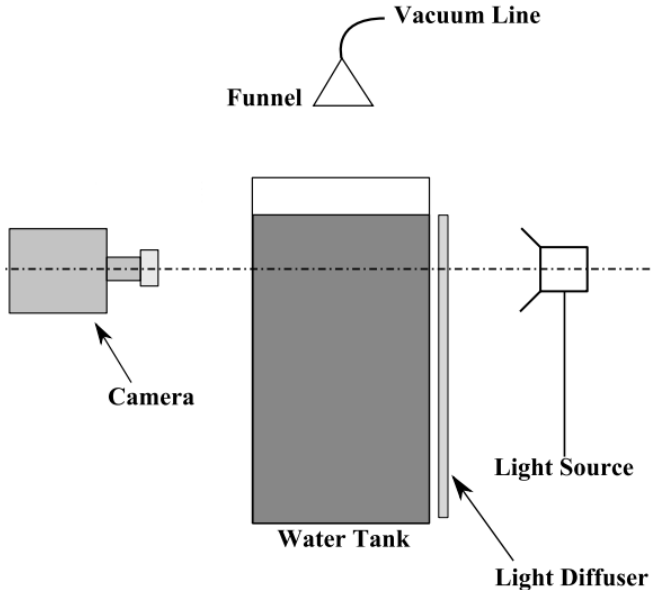

FIG. 2 EXPERIMENTAL SET-UP

A Photron FASTCAM SA1.1 outfitted with a Nikon Nikkor 80-200mm telephoto zoom lens took images of a falling sphere which was backlit using three Lowell DP 1000W lights which were diffused through tracing paper. Pictures with 1024 x 1024 pixel resolution were taken at 5400 frames per second (fps). The field of view in an image was set to capture the entire free-surface impact and cavity pinch-off sequence before the sphere descended out of view. A tank with dimensions of 27.94 cm x 38.1 cm x 76.2 cm was filled with tap water for each of the experiments. A vacuum system was used to hold and release spheres from varying heights (33-214 cm) in order to vary the impact velocity.

Spheres of varying mass were created by adding varying amounts of molten wax and steel shot to a hollow celluloid sphere through a drilled hole. After filling, the hole was plugged with a small stopper and adhesive which was then sanded down to match the contour of the sphere. Two different sphere surface conditions were examined in this study. For one condition, the spheres were washed, thoroughly rinsed with water and dried. In the other condition a hydrophobic coating was utilized. The contact angle of water and sphere for these two surface conditions was determined using the sessile-drop method.

Five spheres were made for each surface condition with mass ratios ranging from 0.66 – 6.78. Water density (ρ_w), viscosity (μ) and surface tension (σ) measurements were taken using a hydrometer, capillary viscometer and DuNuoy tensiometer respectively (Chase Instrument, Cannon #50, CSC-DuNuoy 70535). A precision scale was used to measure sphere mass (m) (Acculab VIC-212) and diameter (D) measurements were made using a micrometer (Mitutoyo). The experimental conditions of this study are listed in Table 1.

TABLE 1 EXPERIMENTAL CONDITIONS

Variable	Value	Units	Uncertainty (%)
ρ_w	998	kg/m^3	1
μ	0.001121	Ns/m^2	2
σ	0.071	N/m	2
Θ	77, 115	degrees	7, 5
D	3.962	cm	0.3
m	21.33 - 220	g	0.3
m*	0.66 – 6.8	-	1
U_o	2.44 - 6.77	m/s	2

To record the position vs. time data from a series of images, a MATLAB program was used. In this program a gray-scale image was converted to a binary image based on an intensity threshold which was determined by the background of the image. The method identified the outline of the sphere and the top-most and bottom-most positions were recorded. The top position was used to determine the impact velocity as the waterline obscured the bottom of the sphere just prior to impact. The bottom of the sphere was used for position data after impact since it was not obscured by the cavity formation or splashing which did affect the algorithm's ability to accurately identify the top position.

It is noted that the pixel-to-meter scaling differed for the sphere in air and in water which was accounted for when converting position measurements from pixels to meters. The sphere position data reported here is measured as the distance from the bottom of the sphere to the height of the undisturbed free surface and time data is reported with time zero coinciding with the time of initial impact.

The instantaneous velocity and acceleration of the spheres after impact was found by fitting a quintic smoothing spline to the position data. This procedure involved the determination of a critical error value to

use for each spline based on the method described by Epps, Truscott & Techet (2010). The purpose of determining this critical error value was to ensure that a smooth curve was fit to the data while also minimizing the deviation between the spline and experimental data. Velocity and acceleration data could then be found as the first and second derivative of the position vs. time spline at each point in time and/or position. Repeated tests were taken for each impact condition and the results reported represent data averaged over multiple trials.

Experimental Results

Cavity Formation and Pinch-off

To characterize the cavity behavior of the impacting sphere, the results were non-dimensionalized. The Weber number based on sphere density was used to capture the density and impact velocity of the spheres,

$$We_s = \frac{\rho_s {U_o}^2 R}{\sigma} \quad (1)$$

where ρ_s is the density of the sphere, U_o is the impact velocity, R is the radius of the sphere, and σ is the surface tension of the water.

The time and depth of cavity pinch-off were examined using a dimensionless depth parameter and two dimensionless time parameters, τ_g and τ_U, used by Truscott, Epps, and Techet (2012), and Aristoff & Bush (2009), respectively. The dimensionless time with respect to gravity,

$$\tau_g = t_p \sqrt{\frac{g}{R}} \quad (2)$$

contains the pinch-off time, t_p, the gravitational acceleration constant, g, and the radius of the sphere, R. The dimensionless time with respect to impact velocity,

$$\tau_U = t_p \frac{U_o}{R} \quad (3)$$

contains the pinch-off time, t_p, the impact velocity, U_o, and the radius of the sphere, R.

For the majority of tests, the non-coated and coated spheres had similar cavity formation results. However, for the lowest impact velocities (2.4 m/s) three of the non-coated spheres failed to produce significant cavities. For the conditions in which cavities were observed, two distinct cavity formations were observed. The majority of the impact conditions yielded a deep seal cavity (Fig. 3A). The 21.3 gram hydrophobic sphere produced a quasi-static cavity for each impact velocity observed (Fig. 3B). The quasi-static cavity is characterized by a pinch-off point occurring on the surface of the sphere. After pinch-off, the quasi-static sphere had very little air attached to it. For the deep seal case an air bubble remained attached to the top of the sphere immediately after pinch-off. It is noted that in comparison with the classification of Aristoff and Bush (2009), the vertical extent of the quasi-static cavity was much greater than the capillary length defined as $l_c = \sqrt{\sigma/\rho g}$.

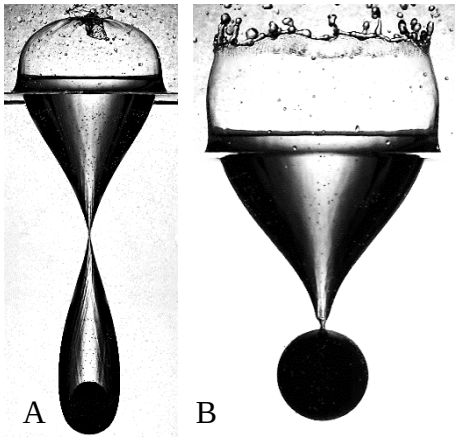

FIG. 3: IMAGES SHOWING PINCH-OFF FOR (A) DEEP SEAL CAVITY AND (B) QUASI-STATIC CAVITY.

The pinch-off depth (z_P) is the distance from the bottom of the sphere to the undisturbed free-surface at the time of cavity pinch-off. Figure 4 reveals the effects of impact velocity and mass ratio on the pinch-off depth. Only the data for hydrophobic spheres is shown, though the non-coated spheres resulted in similar behavior. Increasing the impact velocity and/or mass ratio resulted in a deeper pinch-off depth. It is noted that the effect of increasing impact velocity on pinch-off depth increases with mass ratio. For a mass ratio of 0.66, increasing of the impact velocity from ~2.4-6.2 m/s resulted in a 46% increase in the pinch-off depth while the same increase in impact velocity resulted in a 75% increase in pinch-off depth when the mass ratio was 6.58.

In Fig. 5, the dimensionless pinch-off depth is compared against the impact Weber number based on sphere density. This form of the Weber number captures the kinetic energy of the sphere at impact and a strong correlation can be seen. As the Weber number increases, the dimensionless pinch-off depth increases for cavity-forming cases, with no apparent deviation caused by variation in surface contact angle, sphere density, or impact velocity. The deep seal cavity data follows the same trend as the quasi-static cavity data.

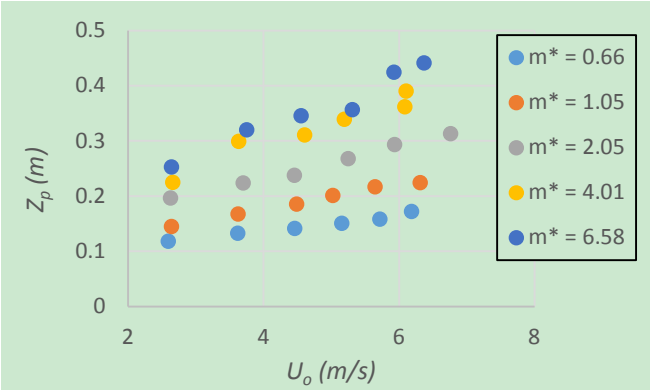

FIG. 4: RELATIONSHIP OF DIMENSIONAL PINCH-OFF DEPTH TO IMPACT VELOCITY AND MASS RATIO (HYDROPHOBIC DATA SHOWN)

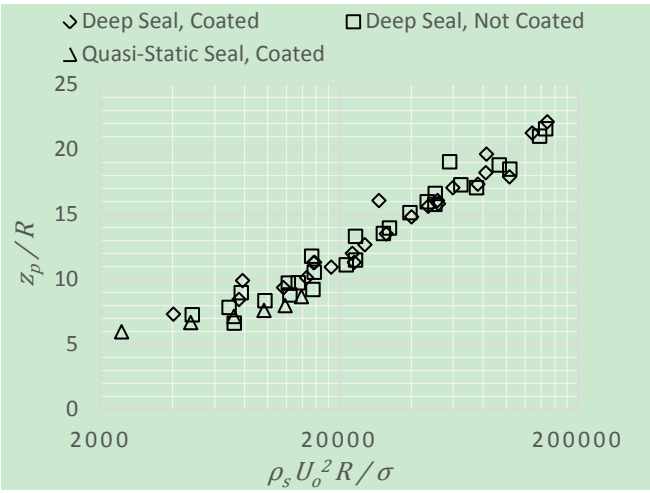

FIG. 5: RELATIONSHIP BETWEEN DIMENSIONLESS PINCH-OFF DEPTH AND WEBER NUMBER

A curve fit to the data for which a cavity formed reveals the following relationship:

$$\frac{z_p}{R} = 0.512\left(\frac{\rho_s U_o^2 R}{\sigma}\right)^{0.337} \quad (4)$$

A comparison of the experimental data with Eq. 4 shows an average deviation of ± 6%.

The dimensionless pinch-off time with respect to gravity appears to be near-constant with respect to the Weber number for all cavity forming cases, as shown in Fig. 6. There is no clear trend showing that the coating or cavity type affects the pinch-off time. From Fig. 6, it is seen that τ_g = 1.807 ± 0.022 for cavity-forming cases. This is in excellent agreement with the deep seal results reported by Truscott, Epps & Techet (2012) of τ_g = 1.78 ± 0.0752.

Figure 7 compares the dimensionless pinch-off time incorporating impact velocity in the Weber number based on the water density. Aristoff and Bush (2009) suggest a linear trend for this comparison (confirmed here as well) and a fit of the current data results in the following relationship:

$$\frac{t_p U_o}{R} = 0.0014\left(\frac{\rho_w U_o^2 R}{\sigma}\right) + 10.502 \quad (5)$$

A comparison of the experimental data with Eq. 5 shows an average deviation of ± 4%.

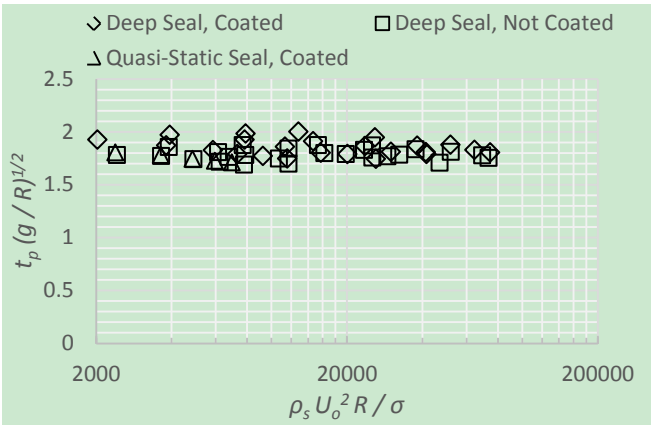

FIG. 6: RELATIONSHIP BETWEEN DIMENSIONLESS PINCH-OFF TIME AND WEBER NUMBER

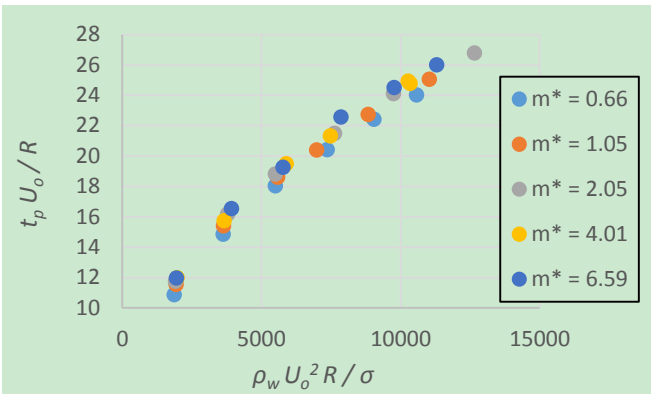

FIG. 7: RELATIONSHIP BETWEEN DIMENSIONLESS PINCH-OFF TIME WITH RESPECT TO IMPACT VELOCITY AND WEBER NUMBER (HYDROPHOBIC DATA SHOWN)

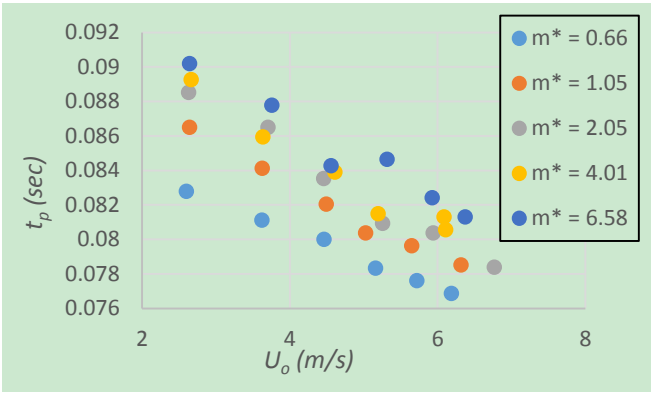

FIG. 8: RELATIONSHIP OF DIMENSIONAL PINCH-OFF TIME TO IMPACT VELOCITY AND MASS RATIO (HYDROPHOBIC DATA SHOWN)

One final analysis was done to elucidate the effect of impact velocity and mass ratio on pinch-off time as

shown in Fig. 8. Increasing the impact velocity and decreasing the mass ratio are both shown to decrease the pinch-off time. For the range of mass ratio conditions studied, increasing the impact velocity from ~2.4-6.2 m/s resulted in a decrease in pinch off time of ~10%. Likewise, for the range of impact velocities studied, increasing the mass ratio from 0.66 to 6.58 resulted in an increase in pinch off time of ~7%.

Acceleration During Impact and Pinch-off

The high-speed camera data was further examined in order to better understand the effect that sphere mass ratio and impact velocity have on the acceleration of the sphere during cavity formation and pinch-off. The large data set will not be provided here in its entirety. For brevity, only a representative selection is shown.

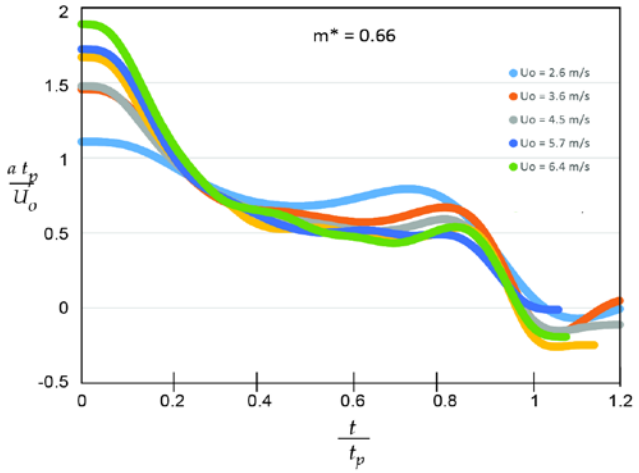

FIG. 9: EFFECT OF VELOCITY ON SPHERE ACCELERATION DURING PINCH-OFF FOR MASS RATIO = 0.66 (HYDROPHOBIC DATA SHOWN)

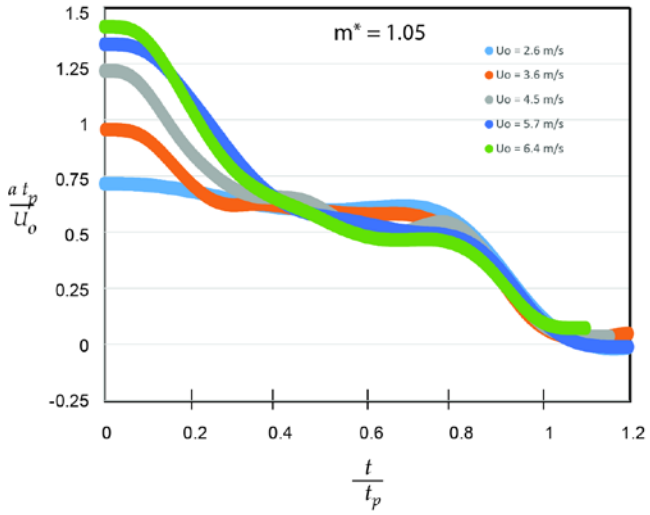

FIG. 10: EFFECT OF VELOCITY ON SPHERE ACCELERATION DURING PINCH-OFF FOR MASS RATIO = 1.05 (HYDROPHOBIC DATA SHOWN)

Figures 9-11 reveal that increasing the velocity while keeping sphere mass constant results in non-dimensional acceleration profiles whose shapes stay relatively similar for a given mass ratio. As the results presented are for data which had a similar cavity (quasi-static or deep seal) this might be expected as the sphere reacts in a similar fashion to the cavity formation and collapse.

It is also seen that acceleration increases with impact velocity for all density ratios. For lower density spheres, this effect is confined to the early entry times.

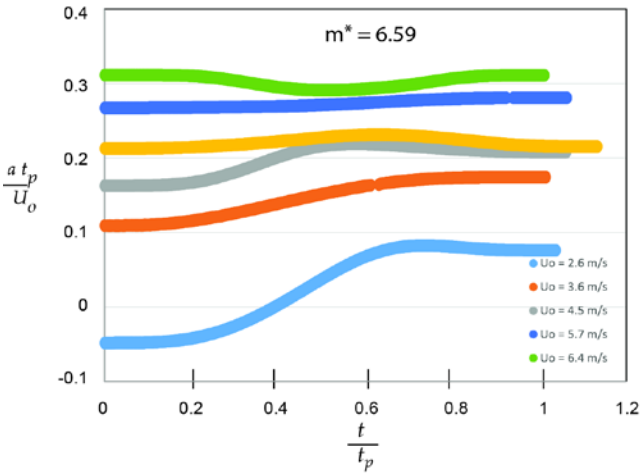

FIG. 11: EFFECT OF VELOCITY ON SPHERE ACCELERATION DURING PINCH-OFF FOR MASS RATIO = 6.59 (HYDROPHOBIC DATA SHOWN)

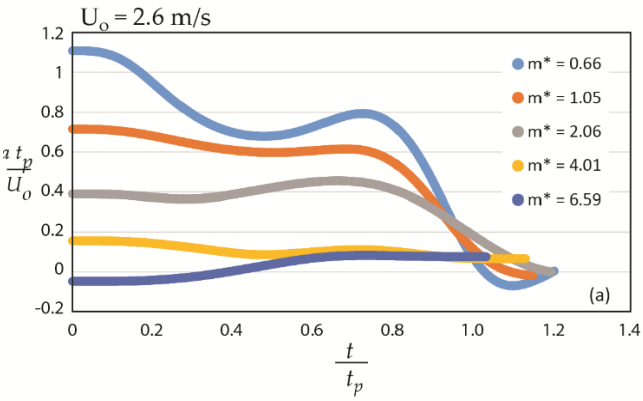

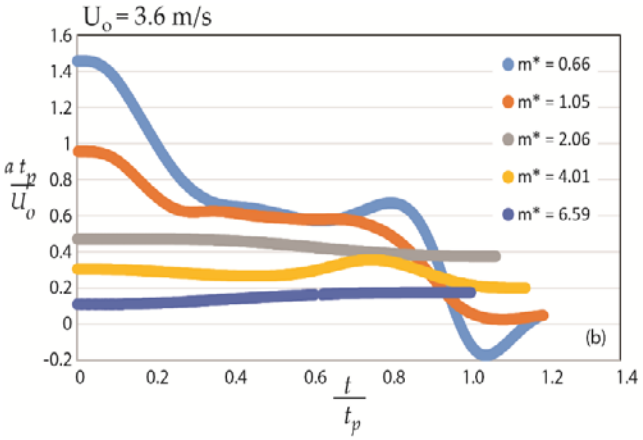

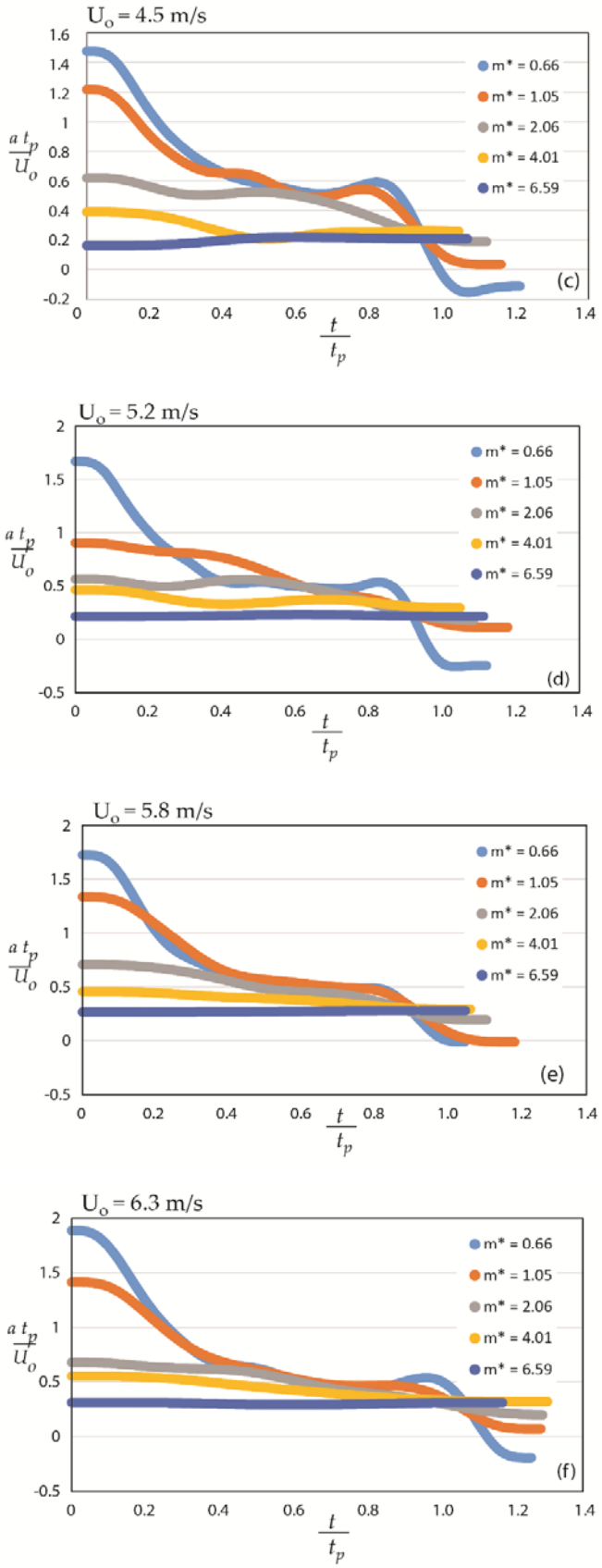

FIG. 12: EFFECT OF SPHERE MASS RATIO ON IMPACT ACCELERATION AT VARYING IMPACT VELOCITIES

The effect of mass ratio on acceleration is shown for different impact velocities in Fig. 12. The effect of mass ratio is significant and was seen to exist for all of the impact velocities examined in this study. Examination of the various mass ratios shows that lighter spheres experience a much higher acceleration and are more affected by the cavity-closure dyanmics. There is a distinct dip in the acceleration curve which occurs just before cavity pinch-off which is in agreement with Truscott, Epps and Techet (2012). The largest mass ratio sphere used in this study shows very little change in acceleration during the cavity pinch-off, especially as impact velocity increases.

Conclusions

In this study, careful experiments have been carried out to assess the impact of surface coating, sphere density, impact velocity on the formation of cavities and on the after-impact acceleration. Experiments covered a nearly three-fold variation in sphere velocity and a ten-fold variation in sphere density. Increasing impact velocity while keeping sphere density constant results in an increase in cavity pinch-off depth and a decrease in pinch-off time. Increasing sphere density while keeping impact velocity constant was shown to result in an increase in cavity pinch-off depth and pinch-off time. When the cavity behavior was recast in dimensionless formats, using a Weber number that incorporated the sphere density, it was found that there was a consistent pinch-off depth/Weber-number relationship which held for both deep-seal and quasi-static cavities. Further investigation showed that there was a remarkable similarity of behavior of the pinch-off time with Weber number (based on liquid density) for spheres regardless of their treatment with a hydrophobic coating for the conditions studied. The similar behaviors encompassed all sphere mass ratios values and for all impact velocities. Finally, the deceleration behaviors were categorized for all impact velocities and sphere mass ratios. Great similarities existed for all cases under investigation.

To the best knowledge of the authors, this study is unique its systematic variation of both impact velocity and mass ratio to carefully document impact deceleration and cavity formation trends for the range of conditions studied. The results of this study will aid in the determination of underwater descent and trajectory of objects which pass from gas to liquid regions

ACKNOWLEDGMENT

The high-speed imaging equipment used during this

research was supported by the National Science Foundation under Grant No. 1229247.

REFERENCES

Abraham, John P., Gorman, John M., Reseghetti, Franco, Trenberth, Kevin and W.J. Minkowycz. "A New Method of Calculating Ocean Temperatures Using Expendable Bathythermographs." Energy and Environment Research 1 (2011): 2-11.

Abraham, John P., Gorman, J., Reseghetti, Franco, Mincowycz, W.J., and Ephraim M. Sparrow. "Turbulent and Transitional Modeling of Drag on Oceanographic Measurement Devices." Computational Fluid Dynamics and its Applications (2012a): doi:10.1155/2012/567864.

Abraham, John P., Gorman, J., Reseghetti, Franco, Sparrow, Ephraim M., and W.J. Mincowycz. "Drag Coefficients for Rotating Expendable Bathythermographs and the Impact of Launch Parameters on Depth Predictions." Numerical Heat Transfer A 62 (2012b): 25-43.

Abraham, John P. et al. "A Review of Global Ocean Temperature Observations: Implications for Ocean Heat Content Estimages and Climate Change." Reviews of Geophysics 51 (2013): 450-483.

Abraham, John P. et al. "Modeling and Numerical Simulation of the Forces Acting on a Sphere During Early-Water Entry." Ocean Engineering 76 (2014): 1-9.

Aristoff, Jeffrey M., and John W.M. Bush. "Water Entry of Small Hydrophobic Spheres." Journal of Fluid Mechanics 619 (2009): 45-78.

Baldwin, John L., and Howard K. Steves. "Vertical Water Entry of Spheres." Technical Report (1975), Naval Surface Weapons Center, Silver Spring, MD, USA.

Duclaux, V., F. Caillé, C. Duez, C. Ybert, L. Bocquet, and C. Clanet. "Dynamics of transient cavities." Journal of Fluid Mechanics 591 (2007): 1-19.

Duez, Cyril, Christophe Ybert, Christophe Clanet, and Lydéric Bocquet. "Making a splash with water repellency." Nature Physics 3 (2007): 180-183.

Epps, Brenden P., Truscott, Tadd T., and Alexandra Techet. "Evaluating Derivatives of Experimental Data Using Smoothing Splines." Proceedings on Mathematical Methods in Engineering International Symposium, Lisbon, Portugal, 2010.

Gorman, John M et al. "Experimental Verification of Drag Forces on Spherical Objects Entering Water." Journal of Marine Biology and Oceanography, 3 (2014): doi:10.4172/2324-8661.1000126.

Lee, M., R. G. Longoria, and D. E. Wilson. "Cavity dynamics in high-speed water entry." Physics of Fluids 9 (1997): 540-550.

May, Albert. "Effect of Surface Condition of a Sphere on Its Water-Entry Cavity." Journal of Applied Physics 22 (1951): 1219-1222.

May, Albert. "Vertical Entry of Missiles into Water." Journal of Applied Physics 23 (1952): 1362-1372.

Stark, John et al. "A Computational Method for Determining XBT Depths." Ocean Sciences 7 (2011): 733-743.

Truscott, Tadd, T., Epps, Brenden P., and Alexandra H. Techet. "Unsteady Forces on Spheres During Free-surface Water Entry." Journal of Fluid Mechanics 704 (2012): 173-210.

Worthington, A. M., and R. S. Cole. "Impact with a liquid surface, Studied by the aid of instantaneous photography." Phil. R. Soc. London A 189 (1897): 137-148.